ARTICLE

PEG-Mediated Synthesis of Highly Dispersive Multifunctional Superparamagnetic Nanoparticles: Their Physicochemical Properties and Function *In Vivo*

Conroy Sun,[†] Kim Du,[‡] Chen Fang,[†] Narayan Bhattarai,[†] Omid Veiseh,[†] Forrest Kievit,[†] Zachary Stephen,[†] Donghoon Lee,[§] Richard G. Ellenbogen,[⊥,∥] Buddy Ratner,[‡] and Miqin Zhang[†,§,⊥,*]

[†]Department of Materials Science & Engineering, [‡]Department of Bioengineering, [§]Department of Radiology, and [⊥]Department of Neurological Surgery, University of Washington, Seattle, Washington 98195, and [∥]Seattle Children's Hospital & Regional Medical Center, Seattle, Washington 98105

ABSTRACT Multifunctional superparamagnetic nanoparticles have been developed for a wide range of applications in nanomedicine, such as serving as tumor-targeted drug carriers and molecular imaging agents. To function *in vivo*, the development of these novel materials must overcome several challenging requirements including biocompatibility, stability in physiological solutions, nontoxicity, and the ability to traverse biological barriers. Here we report a PEG-mediated synthesis process to produce well-dispersed, ultrafine, and highly stable iron oxide nanoparticles for *in vivo* applications. Utilizing a biocompatible PEG coating bearing amine functional groups, the produced nanoparticles serve as an effective platform with the ability to incorporate a variety of targeting, therapeutic, or imaging ligands. In this study, we demonstrated tumor-specific accumulation of these nanoparticles through both magnetic resonance and optical imaging after conjugation with chlorotoxin, a peptide with high affinity toward tumors of the neuroectodermal origin, and Cy5.5, a near-infrared fluorescent dye. Furthermore, we performed preliminary biodistribution and toxicity assessments of these nanoparticles in wild-type mice through histological analysis of clearance organs and hematology assay, and the results demonstrated the relative biocompatibility of these nanoparticles.

KEYWORDS: iron oxide nanoparticle · nanomedicine · cancer · MRI · optical imaging · targeting · chlorotoxin · PEG

Iron oxide nanoparticles have been investigated extensively for biomedical applications such as tumor-specific cell targeting,[1−3] lymph node imaging,[4] visualization of RNA interference,[5] T-cell-specific labeling,[6] inhibition of tumor cell invasion,[7] and stem cell tracking,[8] due to their unique superparamagnetic property and biocompatibility.[9,10] Despite significant advances made in nanotechnology over the past several years, challenges remain in fabricating and processing nanoparticles that are suitable for *in vivo* applications; notably, the issues of particle agglomeration, uniformity, biocompatibility, and tissue-specific targeting must be addressed. These challenges become more outstanding as nanoparticles are further scaled down in size. The high surface area-to-volume ratio of these nanoparticles results in a tendency to aggregate and absorb plasma proteins upon intravenous injection, leading to rapid clearance by the reticuloendothelial system (RES).[11,12] Thus, nanoparticles are commonly protected with a polymer coating to improve their dispersity and stability. Commonly investigated polymers for this purpose include poly(vinyl alcohol) (PVA),[13] poly(D,L-lactide-*co*-glycolide) (PLGA),[14] dextran,[15] poly(ethylene glycol) (PEG),[16] and chitosan.[10,17] Currently, only dextran-coated iron oxide particles (*e.g.*, Ferridex I.V. and Combidex) have made their way into clinical applications. However, these magnetic resonance (MR) imaging contrast agents lack biological targeting or chemical functionality, but rather exploit RES-mediated passive targeting to accumulate in the tissues of interest. The next generation of actively targeting tissue-specific and molecular imaging nanoparticles will require a nanoparticle platform with a long serum half-life and the ability to conjugate various biological molecules.[9]

One of the most promising coating materials for such purposes is PEG because of its ability to provide a steric barrier to protein adsorption, which results in reduced uptake by macrophages of the RES[16] and, ultimately, increased serum half-life.[11] However, PEGylation of iron oxide nanoparticles is often complex involving laborious and sophisticated processes, where minute variations can re-

*Address correspondence to mzhang@u.washington.edu.

Received for review January 31, 2010 and accepted March 9, 2010.

Published online March 16, 2010. 10.1021/nn100190v

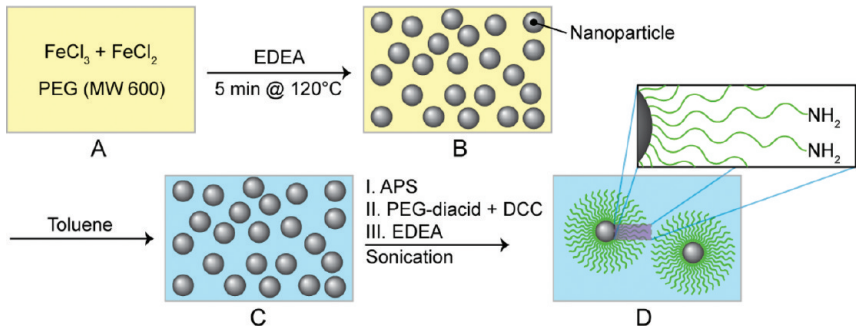

Figure 1. PEG-mediated synthesis schematic of PEGylated iron oxide nanoparticles (ION). (A) Ferrous and ferric chloride dissolved in PEG (MW 600) with 2,2-(ethylenedioxy)bis(ethylamine) (EDEA) under a N_2 environment. (B) High-temperature precipitation of ION at 120 °C. (C) Solvent exchange to replace PEG with toluene. (D) Sequential surface modification of ION with (3-aminopropyl)trimethoxysilane (APS), PEG-diacid, and EDEA to form amine-functionalized ION/PEG.

sult in significant effects on coating efficiency as well as the resultant dispersity of the nanoparticles. PEGs with ability for subsequent conjugation of targeting ligands have been covalently or ionically linked to iron oxide nanoparticles using silane coupling agents in an organic solvent[18,19] or a ligand-exchange strategy to displace hydrophobic surfactants formed on the nanoparticles during particle synthesis.[20,21] The solvent- and ligand-exchange processes are usually time-consuming, exchange efficiencies can vary vastly, and complete removal of the hydrophobic surfactants is difficult.[22] The remaining solvents or surfactants may result in opsonization *in vivo* and other potential side effects, and thus the related biocompatibility issue needs to be addressed.

In this study, we present a simple and yet efficient technique to synthesize highly dispersed ultrafine PEGylated iron oxide nanoparticles (ION/PEG) tailored with the physical and chemical properties necessary for *in vivo* applications. The process utilizes a low molecular weight PEG (MW 600) solution as a high boiling point solvent to control the nucleation and growth of iron oxide cores from iron chloride salts and to provide a steric barrier preventing agglomeration during particle synthesis and subsequent surface modifications. Using chlorotoxin (CTX) as a model targeting agent conjugated on the nanoparticle, we evaluated the efficacy of this nanoparticle system to serve as a targeting contrast agent for both MR and optical imaging *in vitro* and *in vivo*. CTX is a peptide originally isolated from the venom of the *Leiurus quinquestriatus* scorpion[23] and has high affinity for tumors of neuroectodermal origin.[24−26] In addition, CTX has been shown to preferentially bind to cells of a wide variety of tumors, including prostate cancer, intestinal cancer, and sarcoma, suggesting a greater applicability of this targeting agent for other forms of cancer.[27] In our previous work, we demonstrated the targeting specificity of CTX-conjugated iron oxide nanoparticles for xenograft glioma tumors.[1,3,28] In this study, the *in vivo* targeting efficacy of nanoparticles synthesized through this unique PEG-mediated synthesis process was evaluated using a gliosarcoma 9L xenograft mouse model. Furthermore, we performed a preliminary biodistribution and toxicity assessment of these nanoparticles in wild-type mice through histological analysis of clearance organs and hematology assay.

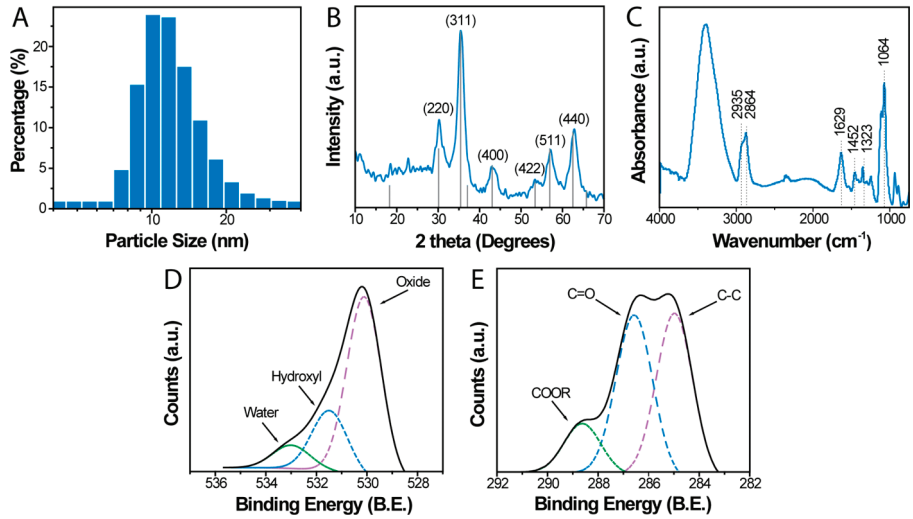

Figure 2. Physical and chemical properties of the ION/PEG. (A) Hydrodynamic size distribution of ION/PEG determined by dynamic light scattering. (B) X-ray diffraction pattern of nanoparticles. (C) FTIR spectrum of ION/PEG. (D,E) XPS spectra of amine-functionalized nanoparticles displaying the O1s (D) and C1s (E) peaks.

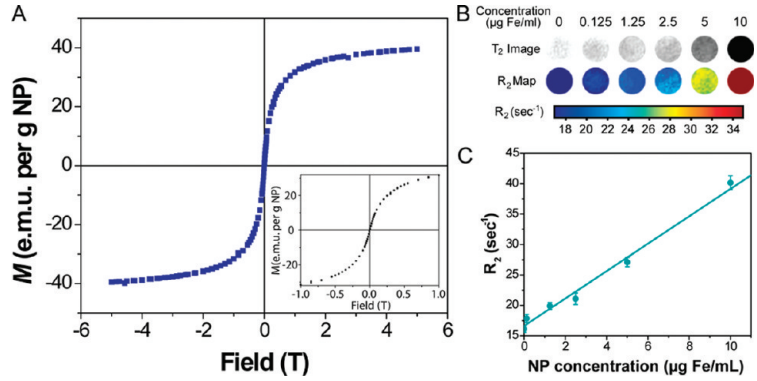

Figure 3. Magnetic properties of the nanoparticle. (A) Magnetization curve of nanoparticles at 300 K. (B) R_2 maps of MRI phantom imaging taken at various nanoparticle concentrations. (C) Relaxation of nanoparticles measured at 4.7 T.

RESULTS AND DISCUSSION

The iron oxide nanoparticles (ION) were synthesized by co-precipitation of $FeCl_2$, $FeCl_3$, and 2,2-(ethylenedioxy)bis(ethylamine) (EDEA) in the presence of PEG (Figure 1A). By using PEG as a high boiling point solvent to control the nucleation and growth of iron oxide cores from iron chloride salts and heating the mixture at a high temperature (120 °C), ultrafine IONs were produced (Figure 1B). The EDEA was utilized as a precipitating agent in this process, as opposed to sodium hydroxide used in many other precipitation procedures where the contamination to the nanoparticle surface by Na^+ ions is a concern. Here, the EDEA adsorbed on the surface of the nanoparticle serves as a coordinating ligand to catalyze, rather than interfere with, the subsequent siloxane surface modification.[29] The PEG solvent was then exchanged with anhydrous toluene (Figure 1C). The nanoparticles in toluene were silanized by introducing (3-aminopropyl)trimethoxysilane (APS) to the reaction mixture to form amine-terminated nanoparticles. The nanoparticles were then grafted with PEG by introducing PEG-diacid into the reaction mixture where the amine-terminated oxide nanoparticles reacted with PEG-diacid to form carboxylic-acid-terminated PEG on the nanoparticles. Finally, amine-terminated PEG on iron oxide nanoparticles (ION/PEG) was formed by addition of EDEA, which reacts with carboxylic-acid-terminated PEG on nanoparticles (Figure 1D). The silanization of nanoparticles with APS, introduced here, renders the nanoparticles much more stable and less susceptible to the changes in synthesis environment (*e.g.*, fluctuations in temperature, type of reactants, and reactant concentrations) than nanoparticles produced by silanization with carboxylic-acid-terminated PEG silane and thus substantially reduces the batch-to-batch variation. This is because small molecules of APS assemble better on nanoparticles than long-chain PEG molecules and thus more effectively shield high-energy surfaces of the oxide nanoparticle, preventing its interactions with other molecules in the solution.

The fate of nanoparticles *in vivo* is strongly dependent on their size and surface chemistry.[30,31] Nanoparticles produced by the PEG-mediated synthesis method were evaluated to determine their physiochemical properties. The hydrodynamic size of the ION/PEG in PBS was determined by dynamic light scattering (DLS). The mean diameter was found to be 13.5 nm with PDI = 0.15 (Figure 2A). This measurement corresponds well with nanoparticle core measurements (4−6 nm) by

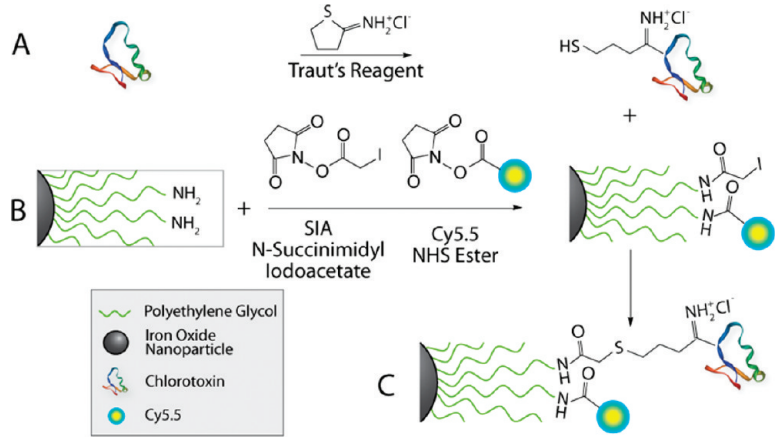

Figure 4. Schematic of CTX and Cy5.5 conjugation to ION/PEG. (A) Thiolation of CTX with Traut's reagent. (B) Iodoacetate and Cy5.5 grafting to amine groups on the ION/PEG *via* NHS esters. (C) CTX and Cy5.5 conjugated ION/PEG.

TEM (Supporting Information, Figure S1). The discrepancy in hydrodynamic size and the core size measured by TEM is due to the hydration of the PEG coating in PBS.

Longitudinal DLS measurements showed no significant particle size change or flocculation in PBS for several months (Supporting Information, Figure S2), demonstrating that these nanoparticles are highly stable and have a suitable shelf life for practical applications. Nanoparticles less than 20 nm in diameter are desirable for most *in vivo* applications to allow for permeation through biological barriers, such as capillary walls and filtering organs.[32] Size reduction also improves the ability of the nanoparticles to evade the detection and clearance by the RES.

The chemical composition and crystal structure of the nanoparticles determined by X-ray diffraction (XRD, Figure 2B) were consistent with that of the inverse spinel structure of magnetite (Fe_3O_4), standard (PDF# 019-0629). The surface chemistry of the ION/PEG was assessed by Fourier transform infrared spectroscopy (FTIR) and X-ray photoelectron spectroscopy (XPS). The IR spectrum of the ION/PEG (Figure 2C) exhibits the characteristics of the amine terminal PEG with methylene signature peaks at 2935 and 2864 cm^{-1} and carbonyl bands at 1629 and 1546 cm^{-1} corresponding to the amide bonds linking the PEG to the silane. In addition, a peak at 1105 cm^{-1} corresponding to the Si−O bond confirms the bonding between the silane and the iron oxide core. A peak at 3400 cm^{-1} corresponds to −OH found on the oxide surface. XPS survey scan spectra showed the presence of Si, C, and O on the nanoparticle surface, confirming the successful deposition of the silane and subsequent PEG grafting (Supporting Information, Figure S3). High-resolution XPS spectra of the O1s (Figure 2D) and the C1s (Figure 2E) display peaks characteristic of the chemical bonds present in the ethylene glycol monomer units of the coating and the iron oxide cores, respectively.

To evaluate the magnetic properties of this nanoparticle platform for MR imaging, samples were examined using a superconducting quantum interference device (SQUID) magnetometer. At 300 K, the ION/PEG demonstrated superparamagnetic behavior displaying a magnetization curve (Figure 3A) with no hysteresis loop. The saturation magnetization (M_s) of ION/PEG was found to be 50 emu/g. In addition, R_2 relaxation was evaluated at 4.7 T by acquiring phantom MR images of agarose samples containing nanoparticles of various concentrations. An R_2 map (Figure 3B) was generated using spin echo images with eight different echo times (T_E) ranging from 13.7 to 170 ms. A linear correlation of R_2 relaxation with iron concentration was established (Figure 3C). The r_2 relaxivity of the ION/PEG was found to be 126.3 s^{-1} mM^{-1}.

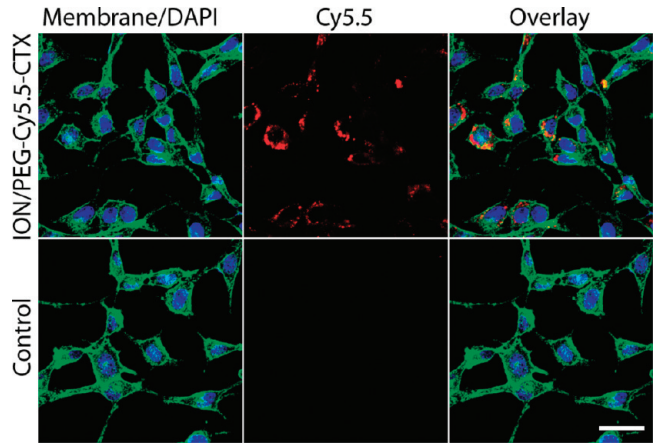

Figure 5. Confocal fluorescence images of 9L cells incubated with 100 μg of Fe/mL ION/PEG-CTX-Cy5.5 for 1 h (top row) and control cells (bottom row). The cellular membranes are highlighted in green, the nuclei in blue, and the NIFR signal associated with the Cy5.5 on nanoparticles is displayed in red. The scale bar corresponds to 30 μm.

To enable and demonstrate the tumor-targeting ability and multifunctionality of this nanoparticle platform, ION/PEG was conjugated with CTX and Cy5.5, as illustrated in Figure 4. To test the functionality of the ligand-attached ION/PEG, an *in vitro* cell uptake assay was performed using 9L gliosarcoma cells.

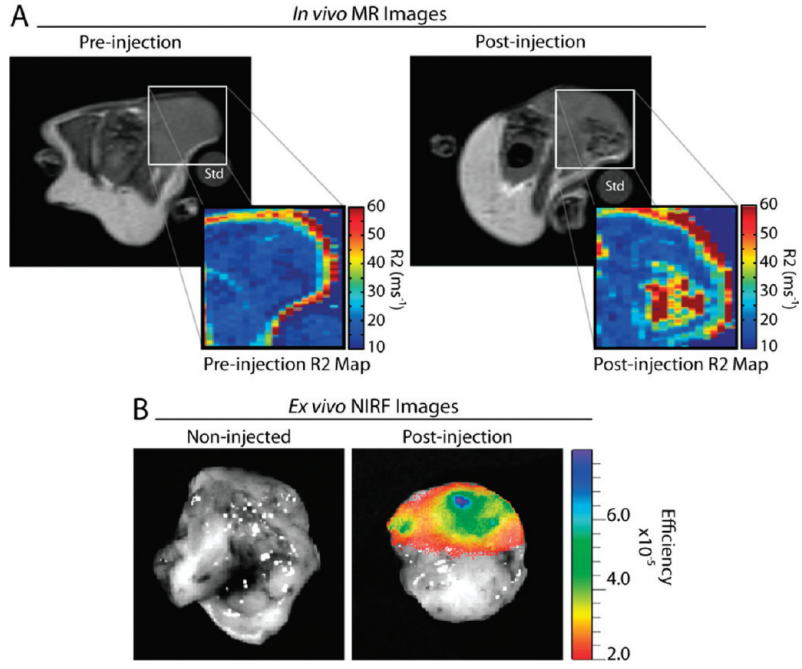

Figure 6. 9L xenograft tumor imaging of mice receiving ION/PEG-CTX-Cy5.5. (A) Representative MRI of the mouse bearing a 9L tumor before and ~48 h after injection of ION/PEG-CTX-Cy5.5 (~10 mg Fe/kg). Heterogeneous accumulation of the nanoparticles as observed by negative contrast enhancement, and R_2 measurement of the region of interest (ROI). A 1% agarose standard (Std) was included to normalize signal intensities between imaging sessions. (B) *Ex vivo* NIRF image of 9L xenograft tumors acquired from a non-injected mouse (left) and the mouse receiving ION/PEG-CTX-Cy5.5 (right) at ~72 h postinjection.

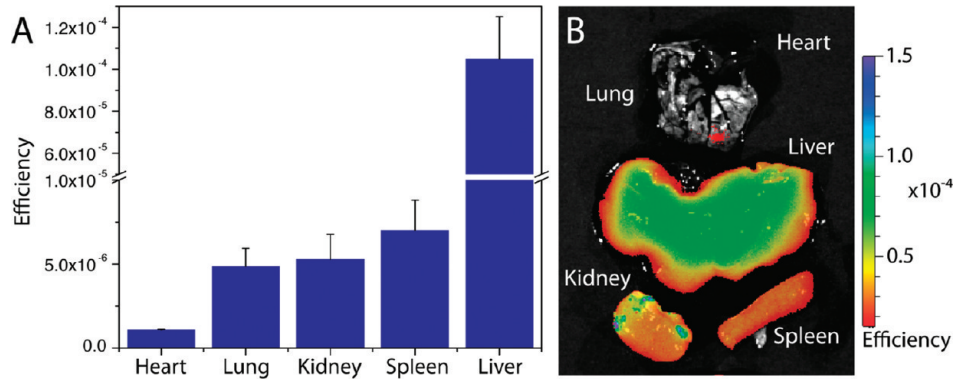

Figure 7. Biodistribution of ION/PEG-CTX-Cy5.5. (A) Relative accumulation of ION/PEG-CTX-Cy5.5 in select tissues of mice ~72 h after injection (~10 mg Fe/kg). Error bars represent standard deviation of measurements from individual animals (n = 3). (B) Representative *ex vivo* NIRF image of mouse tissues after injected with ION/PEG-CTX-Cy5.5.

After 1 h incubation with the nanoparticles at 37 °C, the cells were examined by confocal fluorescence microscopy to observe cell uptake (Figure 5). In these images, the cellular membranes are highlighted in green (TRITC), the nuclei in blue (DAPI), while the NIRF signal associated with the Cy5.5-labeled nanoparticles is displayed in red. The uptake of the ION/PEG conjugated with CTX and Cy5.5 (ION/PEG-CTX-Cy5.5) demonstrates the functionality of these nanoparticles and is consistent with our previous work.[33] These results confirm that the ION/PEG produced by the PEG-mediated synthesis method is suitable for multiple ligand attachment, and the conjugation strategy utilized here may be used for other biomolecules.

The efficacy of the ION/PEG-CTX-Cy5.5 to function *in vivo* (*i.e.*, avoid rapid sequestration by the RES and accumulate in target tumor tissue) was evaluated by MR imaging of tumor-bearing nude mice. In this study, we examined MR contrast enhancement in mice bearing 9L xenograft tumors after administration of ION/PEG-Cy5.5-CTX by tail vein injection (10 mg Fe/kg). MR images were acquired at 4.7 T over a range of echo times (T_E = 14−100 ms) prior to particle injection and 48 h postinjection (Figure 6A). Preinjection images of the tumors illustrated uniform light signal intensity from the tissue area containing the tumor located on the posterior of the animal. Quantitative analysis of these tumors showed R_2 of these tissues in the range of 10−20 ms^{-1} (Figure 6A). MR images of mice injected with the ION/PEG-CTX-Cy5.5 displayed significant contrast enhancement (darkening) heterogeneously throughout the tumor. An R_2 map of the representative image (Figure 6A) illustrates increased R_2 values up to ~60 ms^{-1}, corresponding to the nanoparticle accumulation. The heterogeneous accumulation of these nanoparticles is likely due to the tortuous and poorly defined vasculature of these tumors, which may also contribute to nanoparticle accumulation through the enhanced permeation and retention (EPR) effect.[34,35] The colored R_2 (relaxivity) map of the mouse after injection of ION/PEG-CTX-Cy5.5 further highlights the neoplastic tissue (Figure 6A). Compared to the image of the mouse before nanoparticle treatment, the injection of ION/PEG-CTX-Cy5.5 substantially enhanced the MR contrast of the tumor. These results demonstrate the ability of the nanoparticles to accumulate in targeted tumors.

Furthermore, we utilized NIRF imaging to assess tissue accumulation of ION/PEG-CTX-Cy5.5 in 9L tumor-bearing mice. Here we image in the near-infrared spectral region (600−900 nm) due to low light absorption by physiologically abundant molecules, such as hemoglobin, oxyhemoglobin, and deoxyhemoglobin, allowing for detection of optical tags deep in tissue.[36] Images of tumors were acquired *ex vivo* from non-injected control mice and from mice receiving ION/PEG-CTX-Cy5.5 at 72 h postinjection (Figure 6B). Heterogeneous accumulation of the ION/PEG, consistent with that of the MR images, was evident in the tumors by the significant NIRF signal observed. No fluorescence was observed from the tumors of the non-injected control mice.

We further utilized optical imaging to determine the relative biodistribution of the ION/PEG-CTX-Cy5.5 in wild-type mice through signal quantification of excised tissues 72 h after injection (Figure 7). No significant ION/PEG-CTX-Cy5.5 accumulation was observed in the heart; however, particle accumulation was observed in the lung, kidney, spleen, and liver, as expected. The high hepatic clearance of these nanoparticles is consistent with those reported for other iron oxide nanoparticle systems found in the literature.[5,10,37]

TABLE 1. Liver Enzyme Serum Levels and Complete Blood Counts for Mice Administered with ION/PEG-CTX-Cy5.5 and for Mice Receiving No Injection (as Control)

test	units	ION/PEG-Cy5.5-CTX (mean ± sd)	untreated (mean ± sd)	normal (mean range)
AST	U/L	80 0.0 ± 41.57	72.9 ± 11.1	49.6−171.2
ALT	U/L	47.3 ± 13.0	43.5 ± 12.0	14.1−110.7
WBC	$\times 10^3/\mu L$	6.93 ± 0.12	7.63 ± 2.63	3.56−10.29
RBC	$\times 10^6/\mu L$	11.17 ± 0.54	11.3 ± 0.57	7.59−9.11
hemoglobin	g/dL	15.2 ± 0.8	16 ± 0.8	12.0−14.6
platelet	$\times 10^3/\mu L$	994 ± 384	1096 ± 312	855−2259

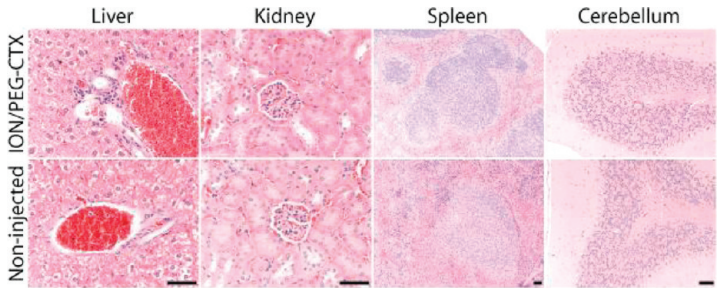

Figure 8. Representative H&E stained tissue sections of mouse liver, kidney, spleen, and cerebellum obtained from non-injected animals (bottom row) and from those injected with ION/PEG-Cy5.5-CTX (10 mg Fe/kg) (top row). No evidence of toxicity was observed in any of the clearance organs. The scale bar corresponds to 50 μm.

A significant concern in the development of new nanomaterials for biomedical applications is the potential for toxicity. To evaluate the biocompatibility of the developed ION/PEG, blood draws were performed on wild-type mice injected with ION/PEG-CTX-Cy5.5 (10 mg Fe/kg) and from control mice receiving no injection. In these assays, healthy wild-type animals were utilized to examine nanoparticle-induced toxicity related to immune response and to avoid possible false malignancies due to tumor-burden. Liver enzyme serum levels and a complete blood count including white blood counts (WBC) and red blood counts (RBC) were measured to detect signs of liver toxicity, anemia, and bone marrow toxicity (Table 1). The hepatotoxicity assay was performed due to the high hepatic clearance of these nanoparticles *in vivo*. Liver enzyme serum levels of mice at 120 h postinjection of ION/PEG-CTX-Cy5.5 showed no significant elevation in aspartate aminotransferase (AST) and alanine aminotransferase (ALT) as compared to the non-injected control mice, and the both AST and ALT levels were within the normal ranges expected for these animals (Table 1).[38,39] These results suggest that administration of ION/PEG-CTX-Cy5.5 did not induce detectable cytotoxic effects on the liver. Measurements of white blood cell count, red blood cell count, hemoglobin levels, and platelet counts were all within normal ranges for healthy animals (Table 1).[40] No appreciable abnormalities in the cell types analyzed were observed, suggesting that the nanoparticles were well-tolerated at the doses evaluated in this study.

Finally, we performed histological analysis on various tissues (kidney, spleen, liver, and cerebellum) of mice injected with ION/PEG-CTX-Cy5.5 to identify any signs of acute toxicity. Tissues were harvested from mice 120 h after receiving particle injection, fixed in 10% formalin, embedded in paraffin, sectioned, and stained with hematoxylin and eosin (H&E). Tissue sections reviewed by a pathologist with expertise in veterinary pathology showed no evidence of toxicity, appearing similar to those observed in the tissues from non-injected control animals (Figure 8).

CONCLUSIONS

Biocompatibility, dispersion, colloidal stability, and targeted delivery have long been scientific and technological challenges in the development of effective nanoparticle-based diagnostic and therapeutic technologies.[41] In this work, we have presented a process for the synthesis of PEG-coated iron oxide nanoparticles and demonstrated their ability to function *in vivo* for applications such as tumor-specific imaging contrast enhancement. This novel synthetic method considerably simplifies nanoparticle synthesis and generates an ultrafine biocompatible ION/PEG system with a hydrodynamic size of ~13.5 nm, an ability to conjugate biomolecules in a modular fashion, and the proper physical and chemical properties suitable for biomedical applications. Through conjugation of CTX and Cy5.5, ION/PEG was shown to specifically accumulate in xenograft tumors of a brain tumor mouse model. Furthermore, results from histopathology and blood toxicity assays indicated that the ION/PEG does not elicit any apparent toxicity or negative health effects.

METHODS

Materials. All materials were purchased from Sigma-Aldrich (St. Louis, MO) unless otherwise specified. Chlorotoxin was obtained from Alomone Laboratories, Ltd. (Jerusalem, Israel). Cy5.5-NHS was purchased from GE Healthcare (Piscataway, NJ).

Nanoparticle Synthesis. Iron oxide nanoparticles were obtained through a PEG-mediated co-precipitation of a 1:2 molar ratio of Fe(II) to Fe(III) with EDEA. Specifically, 0.10 g of $FeCl_2(H_2O)_4$ and 0.16 g of $FeCl_3$ were dissolved in 50 mL of PEG (MW 600). The resulting solution was placed under vacuum overnight at 40 °C to degas the solvent. The mixture was then heated to 125 °C under an inert nitrogen atmosphere. Then, 0.9 mL of DI water was then added, followed by the addition of 10 mL of EDEA. The mixture was then reheated to 125 °C in approximately 5 min. The resulting colloidal solution was destabilized with the addition of toluene to facilitate the magnetic isolation of the nanoparticles. The remaining pellet was washed twice by redispersing the nanoparticles in 200 mL of toluene followed again by magnetic isolation and decanting the supernatant to remove excess PEG and reaction byproducts. The particles were then resuspended in 100 mL of anhydrous toluene prior to the addition of 2 mL of APS for a 12 h silanization reaction at 80 °C. In addition, 400 μL

of titanium(IV) isopropoxide $Ti(OPr)_4$ was added as a catalyst[42] under a nitrogen atmosphere, and the solution was allowed to react under sonication. Excess APS and $Ti(OPr)_4$ were removed by washing the nanoparticles twice with 100 mL of toluene and once with 100 mL of anhydrous toluene. PEG grafting was performed by adding 2 mL of poly(ethylene glycol)bis(carboxymethyl) ether and 1.25 g of *N,N'*-dicyclohexylcarbodiimide (DCC) to the APS-modified nanoparticles redispersed in 200 mL of anhydrous toluene. This mixture was allowed to react under a nitrogen atmosphere in a sonicating bath maintained at 40 °C for 4 h. Ten milliliters of EDEA was then added, and the solution was allowed to react for an additional 4 h under sonication to provide amine terminal groups on the PEG chain. The resulting amine-functionalized PEG-coated nanoparticles were purified by washing three times with ethanol and PBS, respectively. Nanoparticles were stored in a sodium bicarbonate and sodium citrate buffer pH 8.0 at 4 °C and at a concentration of approximately 4 mg Fe/mL prior to further modification.

Nanoparticle Functionalization. CTX and Cy5.5 conjugation to the amine-functionalized nanoparticles was performed using *N*-hydroxysuccinimide (NHS) heterobifunctional linkers and thiolation chemistry. Initially, a sulfhydryl group was formed on the CTX peptide using 2-iminothiolane · HCl (Traut's reagent, Molecular Bioscience, Boulder, CO). A 1:1 molar ratio of Traut's reagent and CTX (500 μg) was combined in 100 mM bicarbonate buffer (pH 8.50) and allowed to react for 1 h at room temperature. Concurrently, 1.0 mg of Cy5.5-NHS and 10 mg of succinimidyl iodoacetate (SIA, Molecular Bioscience, Boulder, CO) were each dissolved into 0.1 mL of dimethyl sulfoxide (DMSO) and then added to the 1.0 mL of the nanoparticle suspension described in the previous section. The solution was protected from light and then placed on a shaker for 2 h at room temperature. The nanoparticles were purified by column chromatography using Sephacryl S-200 resin (GE Healthcare, Piscataway, NJ) eluted with 100 mM bicarbonate buffer (pH 8.50). The 1.0 mg of the purified Cy5.5 and iodoacetate-functionalized nanoparticles (ION/PEG-Cy5.5) were then added to thiolated CTX solution for 2 h reaction at room temperature. Upon conjugation, the Cy5.5- and CTX-conjugated nanoparticles (ION/PEG-Cy5.5-CTX) were purified by column chromatography using PBS to elute through Sephacryl S-200 resin.

Nanoparticle Characterization. Fourier transform infrared (FTIR) spectra were acquired using a Nicolet 5-DXB FTIR spectrometer with a resolution of 4 cm^{-1}. Nanoparticles were lyophilized (Virtis Freezemobile, Gardiner, NY), milled with KBr, and pressed into a pellet for analysis. Powder X-ray diffraction (XRD) patterns were acquired from lyophilized samples with a Philips 1820 X-ray diffractometer using Cu Kα radiation (λ = 1.541 Å) at 40 kV and 20 mA. Hydrodynamic size was measured in PBS using a Zetasizer Nanoseries dynamic light scattering particle size analyzer (Malvern, Worcestershire, UK). X-ray photoelectron spectroscopy (XPS) experiments were carried out at the National ESCA and Surface Analysis Center for Biomedical Problems (NESAC/BIO) at the University of Washington (Seattle, WA). ION/PEG was lyophilized to remove water from samples for analysis. XPS spectra were obtained using a Surface Science Instrument X-probe spectrophotometer with a monochromatized Al X-ray source and 5 eV flood gun for charge neutralization. X-ray spot size for the acquisition was on the order of 800 μm. Pressure in the analytical chamber during spectral acquisition was less than 5×10^{-9} Torr. The takeoff angle was 55°.

Magnetization curves were obtained from lyophilized ION/PEG using a Quantum Design MPMS-5S superconducting quantum interference device (SQUID) magnetometer (Quantum Design, San Diego, CA). *In vitro* MR imaging was performed on a 4.7 T Bruker magnet (Bruker Medical Systems, Karlsruhe, Germany) equipped with Varian Inova spectrometer. A spin echo imaging sequence was utilized to acquire R_2 values at different nanoparticle concentrations ranging from 0.02 to 200 μg Fe/mL. Repetition times (T_R) of 3000 ms were used with echo times (T_E) of 13.7, 20, 40, 60, 90, 120, and 170 ms. The spatial resolution parameters were as follows: an acquisition matrix of 256 × 128, field of view of 40 × 40 mm, section thickness of 1 mm, and 2 averages.

***In Vitro* Fluorescence Microscopy of ION/PEG Uptake.** One million rat gliosarcoma 9L cells (ATCC, Manassas, VA) were plated on 24 mm glass cover slides and grown for 24 h at 37 °C in a humidified atmosphere with 5% CO_2. Cells were washed with PBS and incubated with cell culture medium containing 100 μg of Fe/mL of ION/PEG-Cy5.5 or ION/PEG-Cy5.5-CTX for 1 h at 37 °C. After incubation, cells were washed with PBS three times and fixed in a 4% formaldehyde/PBS solution (methanol free, Polysciences Inc., Warrington, PA) for 30 min. The fixative was then removed, and cells were washed again with PBS three times. Cell membranes were then labeled with AlexaFluor 555 wheat germ agglutinin (Invitrogen, Carlsbad, CA) according the manufacturer's instructions. The slides were then mounted with DAPI-containing Prolong Gold antifade solution (Invitrogen Inc., Carlsbad, CA) for cellular nuclei staining and fluorescence preservation. The slides were examined by fluorescence microscopy using a Zeiss LSM 510 Meta confocal fluorescence microscope (Peabody, MA) equipped with 405 nm diode, 458, 488, 514 nm Argon, and 633 nm HeNe laser lines for excitation, and appropriate band-pass filters for collection of DAPI, TRITC, and NIRF emission signals.

***In Vivo* MR and NIRF Imaging.** All mouse studies were conducted in accordance with University of Washington Institutional Animal Care and Use Committee (IACUC) approved protocols. 9L flank xenograft tumors were prepared in athymic (nu/nu) mice as described previously.[3] 9L mice were injected with nanoparticles at 10 mg/kg (n = 3). MR imaging was performed on a 4.7 T Bruker magnet (Bruker Medical Systems, Karlsruhe, Germany) equipped with Varian Inova spectrometer. A pair of mice were placed in a two-mouse holder and inserted into a Varian 6 cm 200 MHz ^{1}H quad RF coil. Proton density-weighted coronal images were acquired using multiecho−multislice pulse sequences with a T_R of 2000 ms and T_E of 14.2 ms. A series of T_2-weighted coronal images were generated by using single echo−multislice pulse sequences with a T_R of 3000 ms and variable T_E values of 14, 20, 40, 60, 80, and 100 ms. The spatial resolution parameters were as follows: acquisition matrix of 256 × 256, field of view of 60 × 30 mm, slice number of 8, slice thickness of 1.5 mm, gap of 0.5 mm, and 2 averages for proton density-weighted images; acquisition matrix of 256 × 128, field of view of 60 × 30 mm, slice number of 8, slice thickness of 1.5 mm, gap of 0.5 mm, and 2 averages for T_2-weighted images. The R_2 maps for the *in vivo* mouse brain imaging were calculated from T_2 maps generated by the above-mentioned method, and the colorized R_2 maps were generated *via* Matlab R2006a (The MathWorks Inc., Natick, MA).

NIRF images of excised tissues were obtained on a Xenogen IVIS Spectrum system (Caliper Life Sciences, Hopkinton, MA). All images were captured using identical system settings, and fluorescence emission was normalized and reported in efficiency.

Histopathological Evaluation and Hematology Assay. Whole organs (liver, kidney, spleen, and brain) of C57BL/6 mice were removed through necropsy and preserved in 10% formalin for 48 h. Tissues were then embedded in paraffin wax, processed for histology, sliced into 5 μm sections, and stained with hematoxylin and eosin (H&E) according to standard clinical pathology protocols. A veterinary pathologist was then consulted to evaluate if any signs of acute toxicity were present in these clearance organs and brain. Blood cell panels and serum aspartate aminotransferase (AST) and alanine aminotransferase (ALT) levels were quantified 120 h after intravenous administration of ION/PEG-Cy5.5-CTX (n = 3) and compared to both mice receiving no injection (n = 3) and normal ranges of levels reported in the literature. Three hundred microliters of blood was drawn from each mouse through retro-orbital bleeds. Samples were then submitted to a veterinary pathology laboratory (Fred Hutchinson Cancer Research Center, Seattle, WA) for analysis.

Acknowledgment. This work was supported by the NIH/NCI grant (R01CA119408). C.S. and O.V. would like to acknowledge the support of NIH Clinical Neuroscience Training Grant (T32NS007144) and Nanotechnology and Physical Science Training Program in Cancer Research (T32CA138312), respectively. We would like to acknowledge the use of MRI facilities of Diagnostic Imaging Sciences Center at Department of Radiology and the TEM at Department of Botany at University of Washington.

Supporting Information Available: TEM analysis of nanoparticles, long-term stability of nanoparticles in PBS, and XPS analysis of nanoparticles. This material is available free of charge *via* the Internet at http://pubs.acs.org.

REFERENCES AND NOTES

1. Veiseh, O.; Sun, C.; Gunn, J.; Kohler, N.; Gabikian, P.; Lee, D.; Bhattarai, N.; Ellenbogen, R.; Sze, R.; Hallahan, A.; *et al.* Optical and MRI Multifunctional Nanoprobe for Targeting Gliomas. *Nano Lett.* **2005**, *5*, 1003–1008.
2. Sun, C.; Sze, R.; Zhang, M. Q. Folic Acid-PEG Conjugated Superparamagnetic Nanoparticles for Targeted Cellular Uptake and Detection by MRI. *J. Biomed. Mater. Res., Part A* **2006**, *78A*, 550–557.
3. Sun, C.; Veiseh, O.; Gunn, J.; Fang, C.; Hansen, S.; Lee, D.; Sze, R.; Ellenbogen, R. G.; Olson, J.; Zhang, M. *In Vivo* MRI Detection of Gliomas by Chlorotoxin-Conjugated Superparamagnetic Nanoprobes. *Small* **2008**, *4*, 372–379.
4. Harisinghani, M. G.; Barentsz, J.; Hahn, P. F.; Deserno, W. M.; Tabatabaei, S.; van de Kaa, C. H.; de la Rosette, J.; Weissleder, R. Noninvasive Detection of Clinically Occult Lymph-Node Metastases in Prostate Cancer. *N. Engl. J. Med.* **2003**, *348*, 2491–2499.
5. Medarova, Z.; Pham, W.; Farrar, C.; Petkova, V.; Moore, A. *In Vivo* Imaging of SiRNA Delivery and Silencing in Tumors. *Nat. Med.* **2007**, *13*, 372–377.
6. Gunn, J.; Wallen, H.; Veiseh, O.; Sun, C.; Fang, C.; Cao, J.; Yee, C.; Zhang, M. A Multimodal Targeting Nanoparticle for Selectively Labeling T Cells. *Small* **2008**, *4*, 712–715.
7. Veiseh, O.; Kievit, F. M.; Gunn, J. W.; Ratner, B. D.; Zhang, M. A Ligand-Mediated Nanovector for Targeted Gene Delivery and Transfection in Cancer Cells. *Biomaterials* **2009**, *30*, 649–657.
8. Lewin, M.; Carlesso, N.; Tung, C. H.; Tang, X. W.; Cory, D.; Scadden, D. T.; Weissleder, R. Tat Peptide-Derivatized Magnetic Nanoparticles Allow *In Vivo* Tracking and Recovery of Progenitor Cells. *Nat. Biotechnol.* **2000**, *18*, 410–414.
9. Sun, C.; Lee, J. S.; Zhang, M. Magnetic Nanoparticles in MR Imaging and Drug Delivery. *Adv. Drug Delivery Rev.* **2008**, *60*, 1252–1265.
10. Veiseh, O.; Sun, C.; Fang, C.; Bhattarai, N.; Gunn, J.; Kievit, F.; Du, K.; Pullar, B.; Lee, D.; Ellenbogen, R. G.; *et al.* Specific Targeting of Brain Tumors with an Optical/Magnetic Resonance Imaging Nanoprobe across the Blood−Brain Barrier. *Cancer Res.* **2009**, *69*, 6200–6207.
11. Weissleder, R.; Bogdanov, A.; Neuwelt, E. A.; Papisov, M. Long-Circulating Iron Oxides for MR Imaging. *Adv. Drug Delivery Rev.* **1995**, *16*, 321–334.
12. Widder, K. J.; Morris, R. M.; Poore, G.; Howard, D. P.; Senyei, A. E. Tumor Remission in Yoshida Sarcoma-Bearing Rats by Selective Targeting of Magnetic Albumin Microspheres Containing Doxorubicin. *Proc. Natl. Acad. Sci. U.S.A.* **1981**, *78*, 579–581.
13. Lin, H.; Watanabe, Y.; Kimura, M.; Hanabusa, K.; Shirai, H. Preparation of Magnetic Poly(vinyl alcohol) (PVA) Materials by *In Situ* Synthesis of Magnetite in a PVA Matrix. *J. Appl. Polym. Sci.* **2003**, *87*, 1239–1247.
14. Lee, S. J.; Jeong, J. R.; Shin, S. C.; Kim, J. C.; Chang, Y. H.; Lee, K. H.; Kim, J. D. Magnetic Enhancement of Iron Oxide Nanoparticles Encapsulated with Poly(D,L-Latide-*co*-Glycolide). *Colloids Surf. A* **2005**, *255*, 19–25.
15. Shen, T.; Weissleder, R.; Papisov, M.; Bogdanov, A.; Brady, T. J. Monocrystalline Iron-Oxide Nanocompounds (MION)—Physicochemical Properties. *Magn. Reson. Med.* **1993**, *29*, 599–604.
16. Zhang, Y.; Kohler, N.; Zhang, M. Q. Surface Modification of Superparamagnetic Magnetite Nanoparticles and Their Intracellular Uptake. *Biomaterials* **2002**, *23*, 1553–1561.
17. Lee, H. S.; Kim, E. H.; Shao, H. P.; Kwak, B. K. Synthesis of Spio-Chitosan Microspheres for MRI-Detectable Embolotherapy. *J. Magn. Magn. Mater.* **2005**, *293*, 102–105.
18. Kohler, N.; Fryxell, G. E.; Zhang, M. Q. A Bifunctional Poly(ethylene glycol) Silane Immobilized on Metallic Oxide-Based Nanoparticles for Conjugation with Cell Targeting Agents. *J. Am. Chem. Soc.* **2004**, *126*, 7206–7211.
19. Larsen, E. K.; Nielsen, T.; Wittenborn, T.; Birkedal, H.; Vorup-Jensen, T.; Jakobsen, M. H.; Ostergaard, L.; Horsman, M. R.; Besenbacher, F.; Howard, K. A.; *et al.* Size-Dependent Accumulation of Pegylated Silane-Coated Magnetic Iron Oxide Nanoparticles in Murine Tumors. *ACS Nano* **2009**, *3*, 1947–1951.
20. Xie, J.; Xu, C.; Kohler, N.; Hou, Y.; Sun, S. Controlled Pegylation of Monodisperse Fe_3O_4 Nanoparticles for Reduced Non-Specific Uptake by Macrophage Cells. *Adv. Mater.* **2007**, *19*, 3163–3166.
21. De Palma, R.; Peeters, S.; Van Bael, M. J.; Van den Rul, H.; Bonroy, K.; Laureyn, W.; Mullens, J.; Borghs, G.; Maes, G. Silane Ligand Exchange To Make Hydrophobic Superparamagnetic Nanoparticles Water-Dispersible. *Chem. Mater.* **2007**, *19*, 1821–1831.
22. Zhang, T. R.; Ge, J. P.; Hu, Y. P.; Yin, Y. D. A General Approach for Transferring Hydrophobic Nanocrystals into Water. *Nano Lett.* **2007**, *7*, 3203–3207.
23. DeBin, J. A.; Strichartz, G. R. Chloride Channel Inhibition by the Venom of the Scorpion *Leiurus quinquestriatus*. *Toxicon* **1991**, *29*, 1403–1408.
24. Kachra, Z.; Beaulieu, E.; Delbecchi, L.; Mousseau, N.; Berthelet, F.; Moumdjian, R.; Del Maestro, R.; Beliveau, R. Expression of Matrix Metalloproteinases and Their Inhibitors in Human Brain Tumors. *Clin. Exp. Metastasis* **1999**, *17*, 555–566.
25. Deshane, J.; Garner, C. C.; Sontheimer, H. Chlorotoxin Inhibits Glioma Cell Invasion *via* Matrix Metalloproteinase-2. *J. Biol. Chem.* **2003**, *278*, 4135–4144.
26. Lyons, S. A.; O'Neal, J.; Sontheimer, H. Chlorotoxin, a Scorpion-Derived Peptide, Specifically Binds to Gliomas and Tumors of Neuroectodermal Origin. *Glia* **2002**, *39*, 162–173.
27. Veiseh, M.; Gabikian, P.; Bahrami, S. B.; Veiseh, O.; Zhang, M.; Hackman, R. C.; Ravanpay, A. C.; Stroud, M. R.; Kusuma, Y.; Hansen, S. J.; *et al.* Tumor Paint: A Chlorotoxin: Cy5.5 Bioconjugate for Intraoperative Visualization of Cancer Foci. *Cancer Res.* **2007**, *67*, 6882–6888.
28. Sun, C.; Fang, C.; Stephen, Z.; Veiseh, O.; Hansen, S.; Lee, D.; Ellenbogen, R. G.; Olson, J.; Zhang, M. Tumor-Targeted Drug Delivery and MRI Contrast Enhancement by Chlorotoxin-Conjugated Iron Oxide Nanoparticles. *Nanomedicine* **2008**, *3*, 495–505.
29. Kanan, S. A.; Tze, W. T. Y.; Tripp, C. P. Method to Double the Surface Concentration and Control the Orientation of Adsorbed (3-Aminopropyl)dimethylethoxysilane on Silica Powders and Glass Slides. *Langmuir* **2002**, *18*, 6623–6627.
30. Tartaj, P.; Morales, M. D.; Veintemillas-Verdaguer, S.; Gonzalez-Carreno, T.; Serna, C. J. The Preparation of Magnetic Nanoparticles for Applications in Biomedicine. *J. Phys. D* **2003**, *36*, R182–R197.
31. Fang, C.; Zhang, M. Q. Multifunctional Magnetic Nanoparticles for Medical Imaging Applications. *J. Mater. Chem.* **2009**, *19*, 6258–6266.
32. MNneil, S. E. Nanotechnology for the Biologist. *J. Leukocyte Biol.* **2005**, *78*, 585–594.
33. Veiseh, O.; Gunn, J. W.; Kievit, F. M.; Sun, C.; Fang, C.; Lee, J. S.; Zhang, M. Inhibition of Tumor-Cell Invasion with Chlorotoxin-Bound Superparamagnetic Nanoparticles. *Small* **2009**, *5*, 256–264.
34. Maeda, H.; Wu, J.; Sawa, T.; Matsumura, Y.; Hori, K. Tumor Vascular Permeability and the EPR Effect in Macromolecular Therapeutics: A Review. *J. Controlled Release* **2000**, *65*, 271–284.
35. Maeda, H. The Enhanced Permeability and Retention (EPR) Effect in Tumor Vasculature: The Key Role of Tumor-Selective Macromolecular Drug Targeting. *Adv. Enzyme Regul.* **2001**, *41*, 189–207.
36. Frangioni, J. V. *In Vivo* Near-Infrared Fluorescence Imaging. *Curr. Opin. Chem. Biol.* **2003**, *7*, 626–634.

37. Moore, A.; Marecos, E.; Bogdanov, A., Jr.; Weissleder, R. Tumoral Distribution of Long-Circulating Dextran-Coated Iron Oxide Nanoparticles in a Rodent Model. *Radiology* **2000**, *214*, 568–574.
38. Loeb, W. F.; Das, S. R.; Harbour, L. S.; Turturro, A.; Bucci, T. J.; Clifford, C. B. Pathobiology of the Aging Mouse. In *Clinical Biochemistry*; Mohr, U., Dungworth, D. L., Capen, C. C., Carlton, W. W., Sunderberg, J. P., Ward, J. M., Eds.; ILSI Press: Washington DC, 1996; Vol. I, pp 3−19.
39. Wolford, S. T.; Schroer, R. A.; Gohs, F. X.; Gallo, P. P.; Brodeck, M.; Falk, H. B.; Ruhren, R. Reference Range Database for Serum Chemistry and Hematology Values in Laboratory Animals. *J. Toxicol. Environ. Health* **1986**, *18*, 161–188.
40. Jain, N. C. *Vetrinary Hematology*; Lea & Febiger: Philadelphia, PA, 1993.
41. Butterworth, M. D.; Illum, L.; Davis, S. S. Preparation of Ultrafine Silica- and PEG-Coated Magnetite Particles. *Colloids Surf. A* **2001**, *179*, 93–102.
42. Arkles, B. *Silane Coupling Agents: Connecting Across Boundaries V2.0*. Gelest, Inc.: Morrisville, PA, 2006; p 56.